Bluff Body Flow and Noise Control Using Porous Media

Syamir A. Showkat Ali*, X. Liu†and M. Azarpeyvand‡
Department of Mechanical Engineering, University of Bristol, BS8 1TR, UK

This research is concerned with the application of porous materials for reducing noise from bluff bodies by stabilizing the vortex shedding and the wake region. To better understand the noise generation and reduction mechanism, steady and unsteady flow measurements have been carried out. Measurements have been performed for unsteady aerodynamics forces, wake velocity fields and frequency energy content of the turbulent structures within the wake. The study is performed using several types of porous materials, with different porosities and permeability constants and over a wide range of Reynolds number. Results show that the use of a porous cover leads to the reduction of drag in every case of square cylinder, but an increase in drag coefficient in the case of circular cylinder at high Reynold numbers. The effect of porous material on the fluctuating lift force has also been investigated and it has been shown that the lift fluctuations can be reduced significantly using porous covers at low frequencies. The PIV results have also shown that the porous cover can delay the vortex shedding and significantly increase the vortex formation length, leading to a very low turbulent near wake region. It has also been observed that the turbulent kinetic energy in the near wake region can be reduced significantly using the porous layer. These findings are particularly important in the case of noise from tandem cylinder configurations where the wake interaction is the primary source of noise.

Nomenclature

D	cylinder diameter
L	cylinder length
AR	aspect ratio of the cylinder, (L/D)
PPI	pores per inch
μ	fluid viscosity
K	permeability
α	μ/K
β	Forcheimer coefficient
ρ	density of air
W	wind tunnel width
H	wind tunnel height
BR	blockage ratio
C_D	drag force coefficient
C_L	lift force coefficient
f_v	vortex shedding frequency
U_o	free stream velocity
St	Strouhal number, $f_v D/U_o$
Re	Reynolds number
$\varnothing$	porosity
$f(r_1)$	streamwise correlation
x, y, z	cartesian coordinates

*Ph.D Student, Department of Mechanical Engineering, ss14494@bristol.ac.uk
†Ph.D Student, Department of Mechanical Engineering, xl13182@bristol.ac.uk
‡Senior Lecturer and Royal Academy of Engineering Research Fellow, Mechanical Engineering, m.azarpeyvand@bristol.ac.uk

I. Introduction

The flow over bluff bodies has led to continuous studies over the past decades[1–39] for many applications, from aeroplane landing gears to pipe lines, automobiles, high-rise buildings, oil rig platform, bridges, submarines, ships and etc. Hence, it is important to understand the physics of the flow around these structures, which contributes large engineering benefits and industrial significance. One of the complex flow phenomena that occurs around bluff bodies is vortex shedding. Vortex induced symptoms are undesirable in the real world; they can result in structural vibration, acoustic noise, increased drag, stresses on structures, etc. This significant flow induced noise can be suppressed by controlling the flow over the bluff body.[40] Therefore, it is crucial to control the vortex shedding effectively. Both active and passive methods are currently employed to control this vortex shedding.

The passive control method usually related to the shape optimization or customizing the physical properties of the body, for instance adding control rods,[5,6] serration,[41–45]morphing,[46,47] O-rings,[7] helical wires,[8] dimple,[10,11] hairy flaps,[12] splitter plate,[13,14] longitudinal groove,[15] modifying surface with roughness[23] and etc. Bluff bodies noise reduction by the use porous material has been of prime interest to the researchers over the past few years. Experimental studies conducted by Sueki *et al.*[16] showed that the use of open-cell metal foam wraps for an isolated single circular cylinder can lead to significant noise reduction by stabilizing the vortices and the turbulence structure within the wake region. Bhattacharyya and Singh[1] and Bhattacharrya *et al.*[18] showed that the use of porous wrap leads to significant reduction in drag, control of vortex shedding and dampening of the oscillation compared with a solid cylinder. Further studies by Sobera *et al.*[17] found that on account of a subcritical turbulent flow around a cylinder surrounded by a porous layer with a hydraulic resistance typical for that of textile materials, the flow underneath that porous layer is laminar and periodic. Furthermore, Gozmen *et al.*[19] demonstrated that the unsteady flow downstream of the cylinder is controlled and turbulent forced are reduced. In addition, the outer porous cylinders also have a roll in the reduction of vortex shedding in the wake region for all porosities. The turbulent intensity of the flow is reduced at least 45% by the presence of outer porous cylinder compared to the bare cylinder case. The effects of Reynold number in modifying the generated wake behind the cylinder and its corresponding frequency of vortex shedding have been reviewed in several studies.[35–37] It is of interest that the application of porous material for circular cylinder have increase the size of wake by increasing Reynolds number and the turbulent kinetic energy inside the wake is considerably higher than that of a bare cylinder.[38,39] Jim *et al.*[20] studies on turbulent shear flow behaviour over a mass-neutral permeable wall shows that the friction coefficient increases by up to 40% over, which is associated with the presence of large spanwise rollers and the neutral inviscid shear waves of the mean turbulent profile. Mimeau *et al.*[21] investigation over a two-dimensional semi-circular cylinder using porous interfaces results in the best drag reduction with high permeability on lower and upper edges of the body. Analysis by Vafai and Kim[22] on porous material beneath a fluid layer results in a significant reduction in the frictional drag, control of vorticity and diffusion of both external and internal layers of the porous-fluid interface. Numerical investigations conducted by Bruneau and Mortazavi[24–27] shows that the drag, the lift fluctuation, and the global enstrophy were lessened compared to the solid cylinder. Naito and Fukagata[28] have shown that porous treatments for flow control of a single cylinder are more effective at high Reynolds numbers where the growth of instability in the boundary and shear layers would be delayed by the porous surface and therefore the critical Reynolds number for laminar-to-turbulent transition would be shifted up. Even in the fully turbulent regime, the wide low energy region would be created in the wake and the fluctuations of flow field would be largely eliminated. Naito *et al.*[29] have shown that the vortex shedding can be supressed by porous media at very high Reynold numbers. Furthermore, Liu *et al.*[32] study on the application of porous coatings to reduce noise from an isolated cylinder and compared results with measured data from Sueki.[16] Results have shown that a noise reduction of up to 20 dB can be achieved and the fluid diffuses in the porous layer exhibits a slip velocity on the porous and fluid region interface compared to solid cylinder. It can be observed in the case of porous that the shear layer instability at higher Reynolds number is decreased, vortex shedding is suppressed and the wake is regularized which leads to reduction in aerodynamic noise. Additionally, Liu *et al.*[30] studies on the flow characteristics with the gap region between the two bluff bodies indicated that the overall noise level has been decreased by 12-15 dB due to the stabilization of vortex shedding and turbulence within the gap region. More recently, Liu *et al.*[31] investigated the influence of porous material coating on near wake of a cylinder. The results analysis has shown that the porous material cover has prominently modified the flow characteristic of the near wake of circular cylinder and significantly mitigated the fluctuations of aerodynamic forces from two aspects of frequency and amplitude. It means that the vortex shedding from the bluff body is suppressed.

In this paper, a passive flow control method based on porous material for circular cylinder and square cylinder has been investigated. The study interest in reducing the vortex shedding and noise propagation experienced on both circular and square cylinder. The experimental setup and wind-tunnel tests are described in Sec. II. The results and discussions are detailed in Sec. IV.

II. Measurement Setup

Experiments were performed on two bluff body configurations; a circular cylinder and square cylinder at zero angle of attack. A variety of porous materials have been used in these experiments. Measurements have been performed using Force Balance, Hot-wire Anemometry and Particle Image Velocimetry (PIV).

A. Bluff bodies configuration

The schematic of the circular and square cylinder configurations with the porous coatings are shown in Fig. 1. The maximum diameter and length of the circular and square cylinder is D=101.6 mm and L=710 mm, respectively. The cylinders are fixed horizontally, perpendicular to the flow direction (x axis in Fig. 1). With reference to Fig. 1, the origin of the cylinders coordinate system was taken at the center of the cylinder. End plates are used to avoid three dimensional flow at the cylinder ends and as a result the flow at the midspan of the cylinder approaches a two dimensional flow. The end-plates were built in a rectangular shape (700 mm $\times$ 300 mm) with a sharpened leading edges with angle of 20° and were mounted 2.5D from the leading edge and 4.5D from the trailing edge, similar to the configuration recommended by Stansby.[48] Further work by Fox and West[49] added to this specifying that the aspect ratio of the cylinder must be greater than or equal to seven ($AR \geq 7$) in order to give minimal effect on the vortex shedding pattern. The minimum aspect ratio (AR) for the cylinders are calculated to be 7.0 ($AR = L/D$). The porous materials are mainly characterized by their air flow permeability and volume porosity. The porous sheaths wrapped around the cylinder are polyurethane. Figure 2 shows the circular and square cylinders with and without porous covers. The test dimensions and specification for both circular and square cylinders used in this experiment are listed in Table 1. The porous materials properties, *i.e.* porosity and permeability, are presented in Table 2. A total number of 6 to 10 cases have been examined for different test measurements.

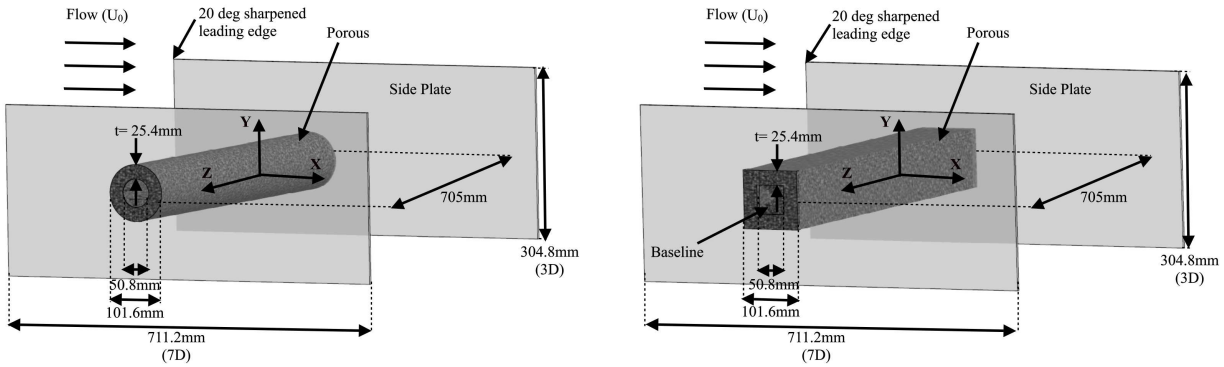

Figure 1: Design configuration(a) circular cylinder and (b) square cylinder with porous cover design configuration with major dimensions and the coordinate axis(an example model of Case 2

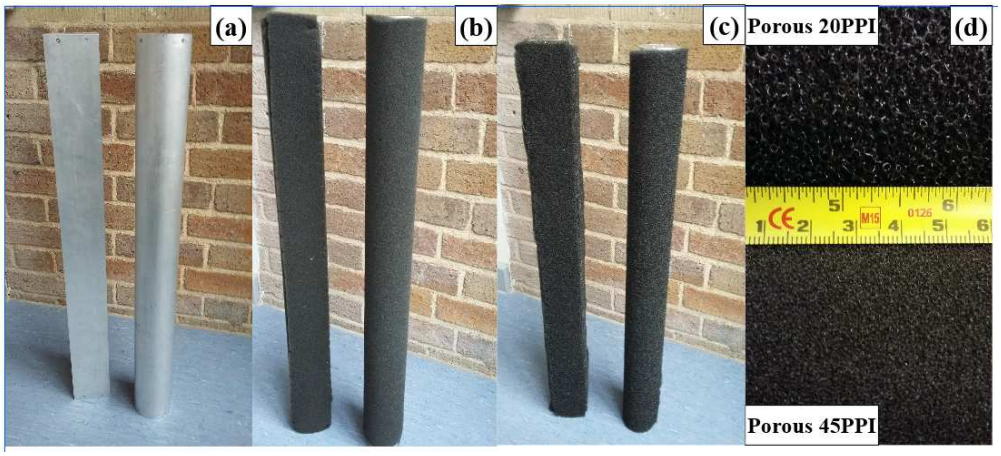

Figure 2: Circular and square cylinders with and without porous cover, (a) solid cylinder, (b) porous 45 PPI, (c) porous 20 PPI and (d) a picture of applied porous materials

Table 1: Circular Cylinder and Square Cylinder Test Design Specification

Geometries	**Cylinder Diameter,** D (mm)	**Porous thickness,** t (mm)	**Pores Per Inch** (PPI)
Solid cylinder	101.6	No	
Case 1	76.2	12.7	20, 45
Case 2	50.8	25.4	20, 45

Table 2: Test Matrix showing the Porosity and Permeability of Samples

Case	PPI	$\varphi(\%)$	$\alpha(Pa\,s/m^3)$	$\beta(Pa\,s^2/m^3)$	$\gamma(m^{-1})$	$K(\times 10^{-6}m^2)$
Solid cylinder	0	0	0	0	0	0
Porous cover, t=12.7mm, 25.4mm	20	92.4	3.079	-0.0523	-0.040	6.440
Porous cover, t=12.7mm, 25.4mm	45	87.9	5.043	-0.132	-0.102	3.932

B. Force Balance Measurements

The aerodynamic lift and drag measurements were performed in the large low speed wind tunnel at the University of Bristol with an octagonal test-section (2.1 m width (W) $\times$ 1.5 m height (H) $\times$ 2.1 m length) with a minimum reliable speed of 10 ms^{-1} and a maximum speed of 60 ms^{-1}. The wind tunnel has a turbulent intensity of 0.25% at 25 ms^{-1}. The wind speed is controlled using a feedback control system and data were recorded when the standard deviation of the velocity was 0.2 ms^{-1} or less. Experimental work has found that the blockage ratios of less than 6 % to have negligible effects on C_D in the subcritical Reynolds regime.[50]The cylinders with porous covers in the tunnel give a blockage ratio of 6.7 % ($BR = (D + t)/H$), which indicates that the blockage ratio will not have significant effect on the drag coefficient. The drag and lift force were recorded using a force balance system. The cylinder was mounted on a steel set of extension arms with symmetrical tear drop shape to minimise any drag or lift generated from them. The extension arms are fixed to an AMTI OR6-7-2000 force balance which was load tested prior to the experiment. The voltage signal obtained from the force balance plate passed through an AMTI MSA-6 strain gauge amplifier and the final data was recorded using a Lab View system. The data is collected for 30 seconds at each velocity with a sampling frequency of 45 Hz for all steady aerodynamic force analysis. The

unsteady lift fluctuations measurement are taken for 3 seconds at each velocity with a sampling frequency of 20,000 Hz, giving a suitably high Nyquist frequency of 10,000. The data have been collected using LabView and imported to MATLAB for data processing. Data were collected from 10 ms^{-1} to 58 ms^{-1} with 2 ms^{-1} increments. This process was carried out for all cylinders and porous cases. Repeat readings were conducted of random porous test cases and solid cylinders in order to ascertain the repeatability of the tests and in all cases, repeat readings were found to be within 1 % of the original data.

C. Particle Image Velocimetry Measurements

The particle image velocimetry (PIV) technique was used to obtain time-averaged velocity and Reynold Stresses over the xy plane. All measurements were performed in the low turbulence wind tunnel at the University of Bristol of closed return type with an octagonal test section (0.8 m width (W) $\times$ 0.6 m height (H) $\times$ 1 m length) with a maximum flow speed of 100 ms^{-1}. The wind tunnel has a turbulent intensity of 0.05 % at 20 ms^{-1}. Two velocity components in real-time velocity maps are measured using a single CCD camera with 2072 x 2072 pixel resolution. The camera was mounted on a traverse system next to the wind tunnel which is in lined with a 210 mm glass window width perpendicular to the laser sheet, and the experiments were carried out at the midplane of the bluff bodies. The time interval and the laser sheet thickness were chosen to attain maximum amount of particles in the interrogation window. The uncertainty is measured by considering the uncertainty in the subpixel displacements[51] and found to be 1 %. A dual-cavity laser of 200 mJ Nd:YAG with a wavelength of 532 nm and 1 mm laser sheet thickness was placed on the bottom of the tunnel and the laser shines through a glass window halfway across the model in a streamwise position. A mixed Polyethylene glycol 80 based seeding was used in the flow, producing particle size from 1 and 5 μm. The time between pulse is fixed in the order of 30 μs with a repetition rate of 10 Hz at U_o= 20 ms^{-1}. The images were processed using a 32 $\times$ 32 rectangular interrogation area with an overlap of 50 %. A total of 1600 image pairs were taken for each case and used to compute the statistical turbulence quantities. The measurements were made for a field view of 190.5 mm $\times$ 190.5 mm, which corresponds to a domain of 2.5 D $\times$ 2.5 D in the streamwise and spanwise directions.

D. Hot-wire Measurements

The steady and unsteady flow and the correlation behind the bluff bodies were measured using a single hot-wire probes. The Dantec 55P16 type sensor with platinum-plated tungsten wire with 5μm wire diameter and 1.25 mm length was used for this purpose. The probe was operated using Dantec Streamline Pro frame with two CTA91C10 modules. The overheat ratio applied for the probe operation is 1.8.[52] The signals obtained were low pass filtered with a corner frequency of 30 kHz before it was A/D converted in order to minimise the effect of low frequency hump due to the open jet shear layer. The data was captured by National Instrument 9215 device. A logging frequency of 40 kHz was used. The measurements were collected for 15 seconds at each measurement locations. The hot-wire probes were calibrated using a Dantec 54H10 type calibrator. Two sets of calibrations were performed before and after each measurement. A traverse system is used to move the hot-wire probe in two perpendicular directions. The traverse unit consists two ThorLabs LTS300M stages with 5 μm accuracy and the unit allowed continuous movement with 300 mm distance in both xy and yz directions.

III. Data Analysis and Post Processing

Porosity ($\varnothing$) is a material property which describes the proportion of the materials volume which is void space. It is defined as the percentage of void volume V_v with respect to the total volume V_t as:

$$\varnothing = \frac{V_t(1 - V_m)}{V_v V_t}, \tag{1}$$

where V_m is the volume of solid material.

Permeability can be defined as the ability of a material to allow a fluid to flow through it. The permeability equation derived by Darcy[53] is defined as:

$$k = \frac{-Q\mu l}{A\Delta P} \tag{2}$$

where Q is the volumetric flow rate, k is the permeability of the material, A is the cross sectional area, ΔP is the pressure difference across the porous medium, μ is the viscosity of the fluid and l is the distance the fluid travels through the porous medium.

The drag coefficient C_D is defined by:

$$C_D = \frac{D}{\frac{1}{2}\rho A U_o^2} \tag{3}$$

where D is the average drag force, ρ is the density of fluid, A is the characteristic area (in this case equal to the area of the cylinder normal to the direction of fluid flow) and U_o is the velocity of the fluid. The arms and side plates provided a considerable contribution to overall drag values recorded for the cylinder despite their aerodynamic properties. To calculate the drag coefficient for the cylinder only, the drag coefficient for the arms and side plates were calculated separately at each velocity and then subtracted from the drag coefficient for the entire rig.

The mean velocity can be obtained from:

$$U_{mean} = \frac{1}{N}\sum_{i=1}^{N} U_i, \tag{4}$$

where N is the total number of velocity samples in time.

The Reynold shear stresses of two simultaneous time series signals can be calculated as:

$$\overline{u'v'} = \frac{1}{N}\sum_{i=1}^{N} (U_i - U_{mean})(V_i - V_{mean})\,. \tag{5}$$

To identify the pattern of turbulent structures in space, two point correlation function of the velocity is used:

$$R_{ii}(r) = \frac{< u_i'(x_i,t)u_i'(x_i+r,t) >}{< (u_i')^2 >}, \tag{6}$$

where u_i' is the fluctuating velocity, r is the distance between two single wires and x_i-coordinate in streamwise direction.

IV. Results and Discussion

To better understand the effect of porous cover on the aerodynamic performance and the flow field, the steady drag force, unsteady lift force and the wake velocity profiles for both circular and square cylinders are presented in this section. Further discussions on the correlations in the streamwise direction is also given here.

A. Steady and Unsteady Measurements on Circular and Square Cylinders

Experiments have been carried out to cover a wide range of Reynolds number: $Re_D = 6.7 \cdot 10^4$ to $3.9 \cdot 10^5$, corresponding to a flow velocity of U_o=10 ms^{-1} to U_o=58 ms^{-1}.

1. Steady drag force results for circular cylinder

The results obtained in Fig. 3 give unique information concerning all cases where the inclusion of porous covers have reduced the C_D for the subcritical regime about the range up to 1.5×10^5. However, contrary to previous numerical and experimental findings,[2,10,11,13] the inclusion of porous covers have universally increased C_D in the critical Reynolds regime in the range of 2×10^5 to 4×10^5 for the circular cylinder. The results presented also suggest that the application of the porous covers of any permeability suppresses the onset of the critical Reynolds regime and thus there is no drop in C_D and it becomes Reynolds independent. Generally, larger porous cover thickness used has the largest increase of the drag performances. More notably, the covers with t=12.7 mm have the least increase in C_D compared to the solid cylinder for all permeability (K) throughout the Reynolds range tested. Similarly, the thickest case t=25.4 mm has the largest increase of C_D, constant for all K. Additionally, the parameter thickness, t is important and directly related to the

increase in C_D. As expected, highly permeable porous media were more efficient in drag reduction. Also, for a constant thickness, porous cover with smaller permeability with 45 PPI has lower drag force drop compared to 20 PPI cover which holds higher permeability value. Between the two covers of higher permeability, the thicker cover has a lower drag coefficient; this directly matches with numerical findings of Bhattacharyya and Singh.[1] Between the two lower permeable covers the thicker cover produces the most drag as the fluid has to pass through more material with higher resistance.[26] Comparing the thickness and permeability of each case, the result suggests that in the critical range, the permeability of the porous cover has a more dominant effect than thickness. Hence, it is apparent that the optimal material properties of K=6.440 $\times$ 10^6 m^2 have been identified to result in the largest reduction in C_D for all $\varnothing$ value relative to the solid cylinder.

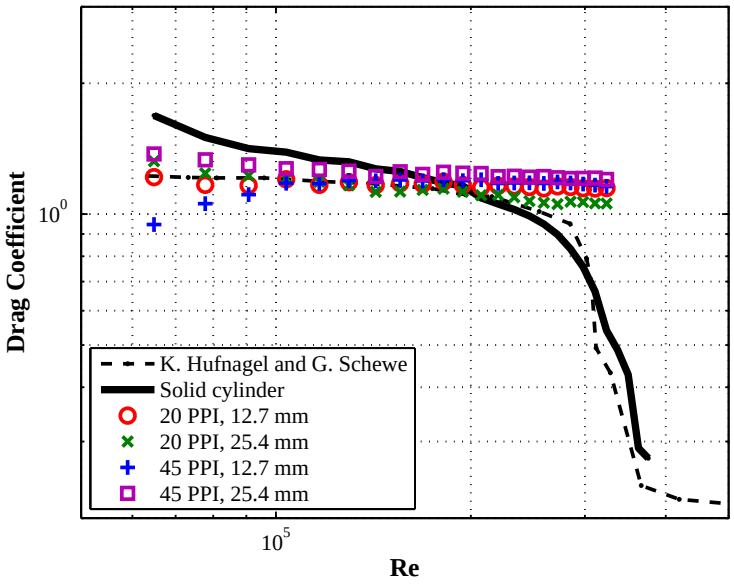

Figure 3: Plots showing trends in C_D in the subcritical and critical regime after application of porous cover for circular cylinder

2. *Steady drag force results for square cylinder*

Figure 4 shows the mean drag force results for a square cylinder with and without porous cover. As expected, the result for the solid square cylinder is found to be independent of the Reynolds number. The trend of the solid cylinder does match the earlier study conducted by Hufnagel and Schewe[54] with only a slight discrepancy at the higher end of the Reynolds range. Results also show that the porous covers generally reduce the drag coefficient. This result had previously been predicted by many of the numerical simulations.[27,55,56] The data obtained has remained fairly consistent across the entire Reynolds region. It has also been found that the entire range of porous materials used has reduced the mean drag force experienced on the square cylinder. Notably, the use of thicker porous covers provides more significant reduction of the drag coefficient. In addition, the drag coefficient undergo significant decrease for porous cover with lower porosity and high permeability, except for the case of cylinder with 12.7 mm, 20PPI which appears to be least effective in the range up to 1.5 $\times$ 10^5 Reynolds number. Moreover, there is a considerable increase of drag in the case of the cylinder with 25.4 mm, 45 PPI above the Reynolds number about 1.7 $\times$ 10^5. It can also been seen that the permeability of the porous coating appears to have a greater effect than the thickness. This conclusion can be made from the fact that the 20 PPI (12.7 mm) case reduces the drag coefficient more than the 45 PPI (25.4 mm) case. Hence, it is apparent that the optimal material properties of thickness, t=25.4 mm and permeability, K= 6.440 $\times$ 10^6 m^2 have been identified to result in the largest reduction of C_D. This is in agreement with the findings of Bruneau *et. al*[27] where porous material, with larger permeability values had significantly reduced C_D.

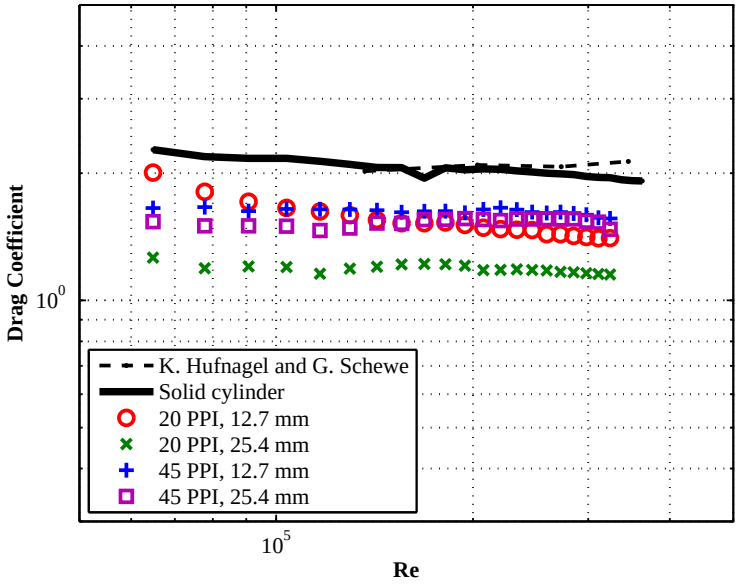

Figure 4: Plots showing trends in C_D in the subcritical and critical regime after application of porous cover for square cylinder

3. Unsteady lift force results for circular cylinder

The unsteady lift fluctuation results for solid and treated cylinders are provided here. The Welch power spectral density estimate has been applied to the time history data recorded from the force plate. In order to evaluate the suppression of fluctuating lift power from the porous cases, the lift power plots are presented to compare porous cases of equal thickness to that of a solid cylinder with $d = D + 2t$ in Figs. 5 and 6. The inclusion of the porous covers have little effect on the lift power at low U_o and therefore have not been presented. At higher velocities, there appears to be significant reduction of the low frequency energy content between 0-100 Hz for both U_o =40 and 50 ms^{-1} and is consistent for both t= 12.7 mm and 25.4 mm. It is clear that the lowest permeability case, K=3.932 $\times$ 10^5 m^2 appears to have the most consistent decrease of lift power at U_o =50 ms^{-1} across the frequency range of interest.

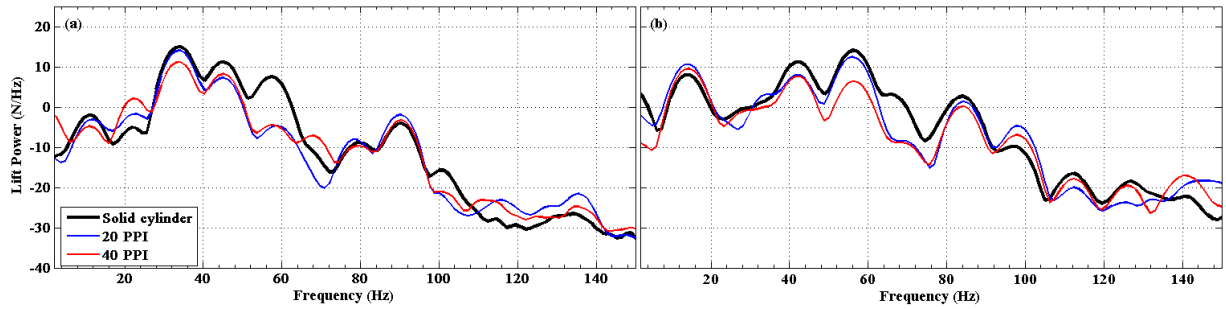

Figure 5: Lift power spectrum for all K and t=12.7 mm at (a) 40 ms^{-1} and (b) 50 ms^{-1}

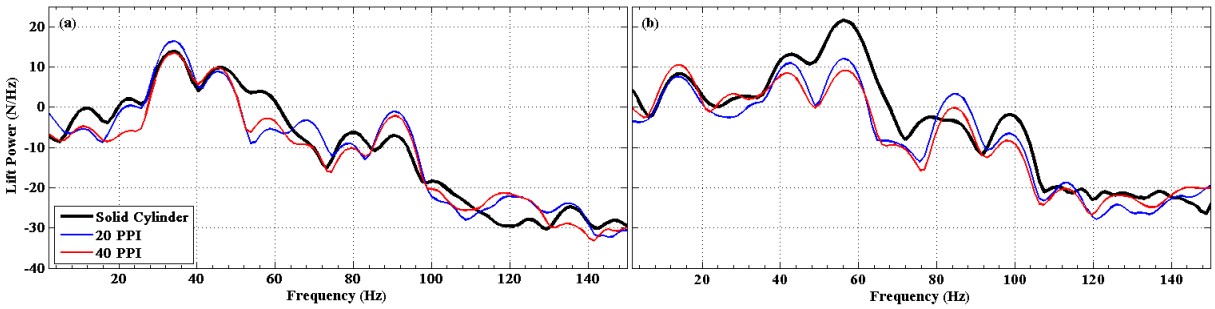

Figure 6: Lift power spectrum for all K and t=25.4 mm at (a) 40 ms^{-1} and (b) 50 ms^{-1}

4. Unsteady lift force results for square cylinder

Figures 7 and 8 show the results for the unsteady lift fluctuations for square cylinders, with and without porous treatment. Results show that there is a significant reduction of the low frequency energy content in the case of porous between 0-80 Hz for both U_o =40 and 50 ms^{-1} and is consistent for all t. At velocities of 40-50 ms^{-1} across all thicknesses the porous material appear to cause a consistent reduction of the oscillating lift force across the entire frequency range presented. It is clear that the highest permeability case, K=6.440 $\times$ 10^5 m^2 appears to have the most consistent decrease of lift power at U_o=50 ms^{-1} across the narrow band frequency range. The different porosities have had very inconsistent and varied degree of success on reducing the lift force power with no value of porosity being obviously more successful than another.

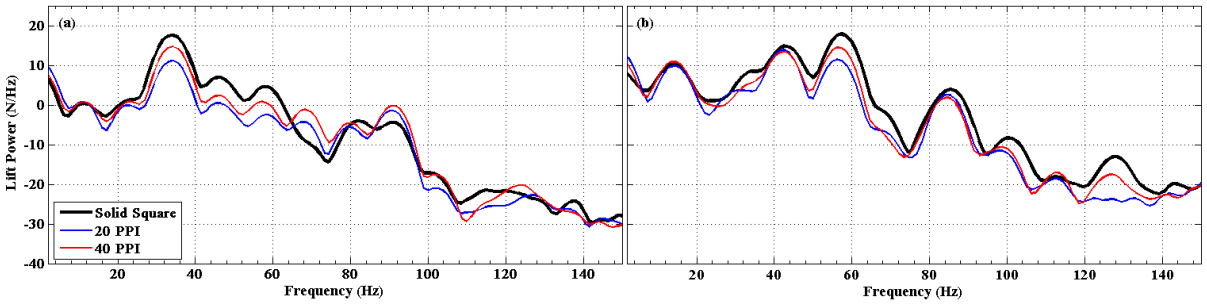

Figure 7: Lift power spectrum for all K and t=12.7 mm at (a) 40 ms^{-1} and (b) 50 ms^{-1}

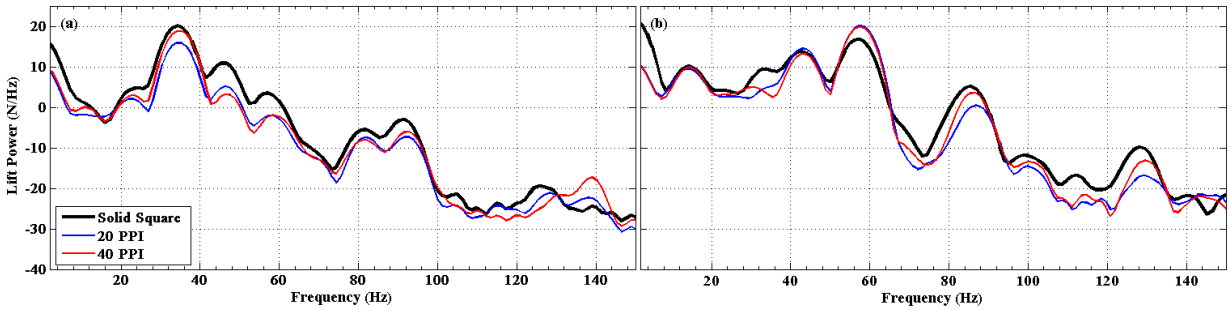

Figure 8: Lift power spectrum for all K and t=25.4 mm at (a) 40 ms^{-1} and (b) 50 ms^{-1}

B. Wake Profile Study

1. *Flow Velocity streamlines for circular and square cylinders*

In order to better understand the effects of the porous covers on the vortex shedding and the wake development, PIV measurements have been carried out at the Reynolds number of $Re_D = 10^5$ corresponding to the flow velocity of U_o =20 ms^{-1}. Figures 9 and 10 show the time-averaged velocity streamline topology for circular and square cylinders with and without porous treatment, respectively. As can be seen, a pair of counter rotating vortices are formed with nearly identical symmetric structure with respect to the centerline.

Result in Fig. 9 (a) shows that, the flow recirculation behind the solid cylinder occurs within $1.5 \lesssim x/D \lesssim 2.6$. The use of porous materials results in moving of the main circulation area to further downstream. This can be seen in Figs. 9 (b) and 9 (c) where the locations of both recirculation occur within $2 \lesssim x/D \lesssim 3.2$ and $1.9 \lesssim x/D \lesssim 3.42$, respectively.

In the case of solid square cylinder, it can be seen from Fig. 10 (a), that the flow recirculation appears at $0.65 \lesssim x/D \lesssim 1.8$. In Figs. 10 (b) and 10 (c), it is clearly noticed that the circulation areas have moved further downstream to $1.8 \lesssim x/D \lesssim 3.2$ and $2.4 \lesssim x/D \gtrsim 3.8$, respectively.

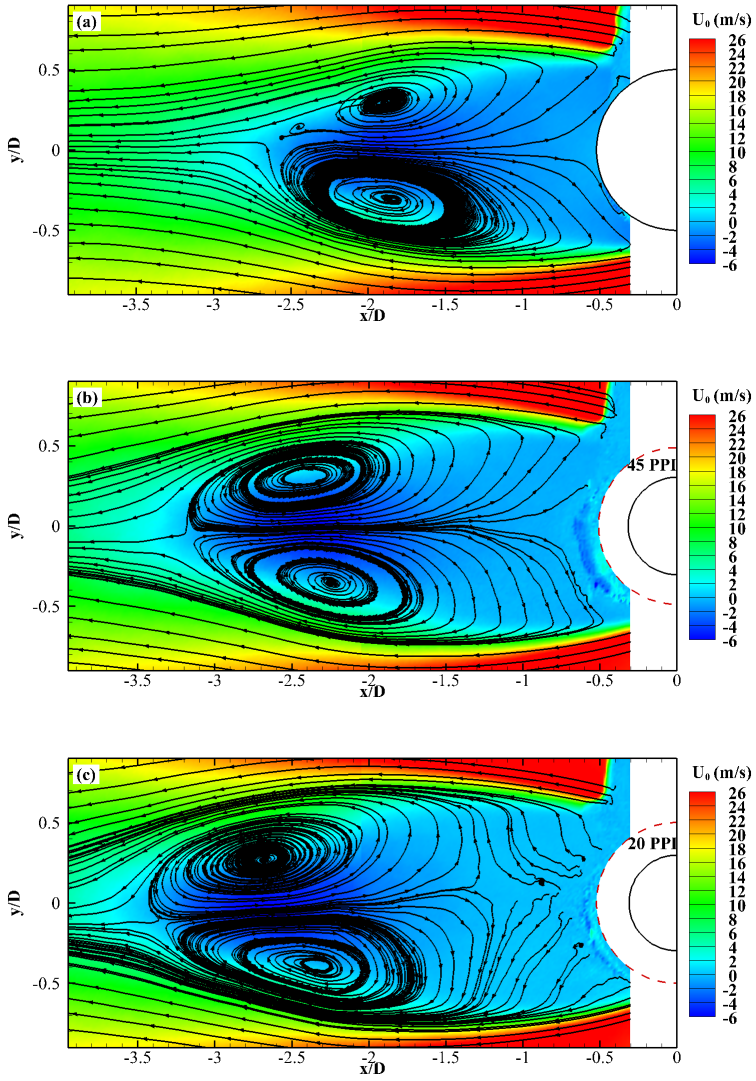

Figure 9: Time-averaged streamline topology for (a) a solid circular cylinder, (b) a circular cylinder covered with 45 PPI porous layer and (c) a circular cylinder covered with 25 PPI porous layer, at U_o =20 ms^{-1}.

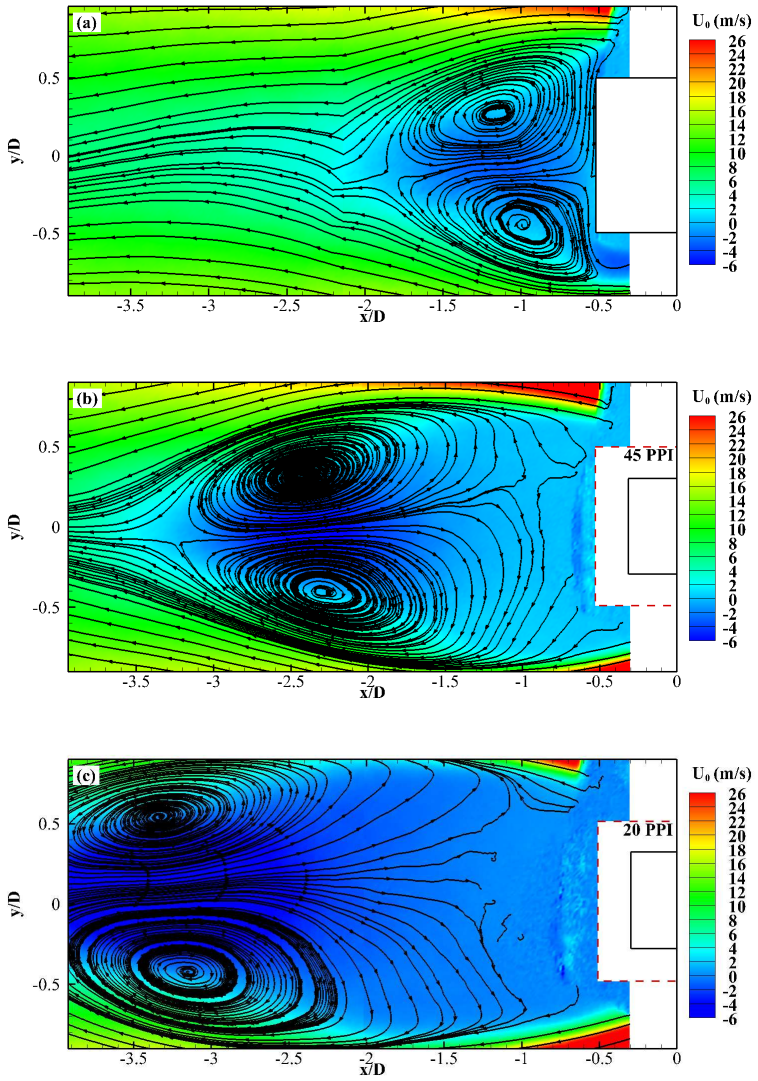

Figure 10: Time-averaged streamline topology for (a) a solid square cylinder, (b) a square cylinder covered with 45 PPI porous layer and (c) a square cylinder covered with 25 PPI porous layer, at U_o =20 ms^{-1}.

2. *Wake Velocity profiles*

The categorization of vortex shedding regimes in the wake velocity profile specifically in the near wake flow can be assessed by looking into the vortex formation length and the mean recirculation region. The vortex formation length is defined as the distance measure from the cylinder center to the end of the vortex region, in which L_f is the point in the wake where maximum velocity fluctuation is obtained and consequently decays downstream.[57] The mean recirculation region on the other hand can be described as the surface where shear stresses and pressure forces are stable in equilibrium stage. The effect of the vortex formation length, L_f and the mean recirculation region can be clearly seen in the streamwise mean velocity plot along the wake centerline and the edge of upper cylinder (lip-line) axis depicted in Figs. 11 and 12, respectively. It can be seen that the magnitude of U/U_o in Fig. 11 initially decreases with distance along the wake centerline axis for both types of cylinders and consequently increases thereafter. The recirculation region is apparent to be more reduced in the porous cases of both circular and square cylinders at $0.5 \lesssim x/D \lesssim 1$ and $0.5 \lesssim x/D \lesssim 1.5$, respectively. Further downstream, the large recirculation region can be seen more clearly in the porous cases for the both types of cylinders. Obviously, results indicate that the recirculation zone and vortex formation are delayed significantly in the presence of porous material which also agrees reasonably well with

the streamline topology figures, where the L_f is relatively larger in the porous cases compared to the solid cylinders. In short, the vortex formation region was pushed further downstream as the direct consequences of porous treatments. The values of the L_f for all the cylinders with and without porous treatment are listed in Table 3. The results presented here reconcile the previous results in Figs. 9 and 10 that the L_f was found to be longer in the case of porous treated cylinders.

Figs. 12 (a) and 12 (b) show the streamline mean velocity plots along the edge lip-line of upper circular and square cylinders, respectively. Both the figures show almost the same trend where the mean velocity increases along the wake axis to a maximum value at some downstream of the cylinders. The distribution of the mean velocity in the case of porous treated cylinders are relatively lower than the solid cylinders. There is a slight variation of the lower velocity range in porous 45 PPI and porous 20 PPI up to $x/D = 2.5$, and subsequently becomes constant at further wake for both types of cylinders. The growth of the shear layer is notably smaller in the porous cases which is due to the increase in velocity gradients and the narrowing of the wake. At $x/D = 0.5$, the shear layer velocity are almost similar for all cases where the wake was stabilized behind the cylinders. These characteristics can also be observed in Figs. 13 and 14. As expected, the accelerated flow at the edge of the shear layer has been altered in the case of porous treated cylinders, resulting in the reduction of the mean velocity in the near wake. The flow which was emitted through small pores from the porous medium leads to the reduction of the velocity fluctuations in the shear layer.

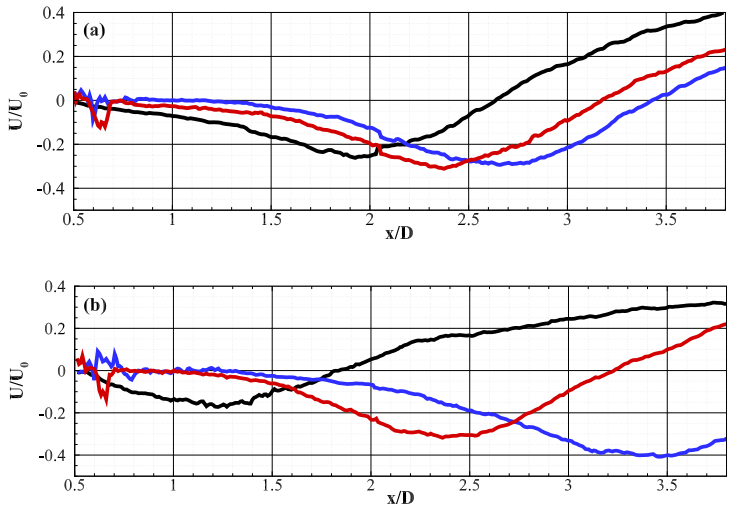

Figure 11: Mean velocities along the wake centerline (a) circular cylinder (b) square cylinder. *Black line: Solid; Blue line: Porous 25 PPI; Red line: Porous 80 PPI*

Table 3: Non dimensional L_f values for circular and square cylinders with and without porous treatments

Test Rig	**Solid Cylinder**	**Porous 25 PPI treated cylinder**	**Porous 20 PPI treated cylinder**
Circular Cylinder, L_f/D	2.63	3.18	3.42
Square Cylinder, L_f/D	1.80	3.20	> 3.80

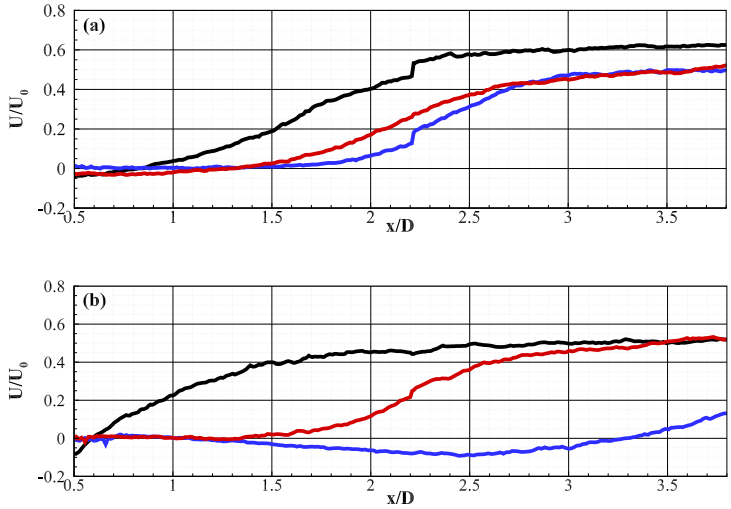

Figure 12: Mean velocities along the edge lip-line of upper cylinder (a) circular cylinder (b) square cylinder. *Black line: Solid; Blue line: Porous 25 PPI; Red line: Porous 80 PPI*

3. Wake velocity profile for circular and square cylinders

Figures 13 and 14 show the wake U and V velocity profiles at different axial locations, x/D=0.5, 1.0, 1.5, 2.0, 2.5 and 3.0, downstream of the cylinder. The locations are selected based on the vortex shedding location. A negative velocity region is visible at all axial locations except at $x/D = 3.0$. The figure illustrates that near the cylinder, the profile behaves like a flat 'top hat' at $x/D = 0.5$ for all measured cases and at $x/D = 1.0$ for porous cases which then steadily becomes narrow at downstream locations. The top hat profiles demonstrate that the flow in the near wake is uniform and having an almost constant velocity region; which is the implication of flow separation from the cylinder surface. It is noticed that the momentum deficit of the porous cases in the near wake ($x/D = 0.5$ and $x/D = 1.5$) is smaller than that of solid case, but larger in the far wake. Particularly, in this case, the solid cylinder profile becomes narrow at $x/D = 1.0$ in the negative velocity region while all porous cases reached negative values at $x/D = 1.5$ and increase from negative values to maxima at $x/D = 3.0$, where no recirculation occurs in this region. The evidence for the support of this result can be found in Fig. 9. The V velocity component in Fig. 14 are more or less symmetric about the wake axis. The V velocity results at $x/D = 0.5$ demonstrate that the velocity gradient are almost similar for all cases in which the flow is stable in that region; the values are principally negative for y < 0 and positive for y > 0. However, at farther downstream, the values are negative for y > 0 and positive for y < 0. This is due to the appearance of the recirculation region and vortex formation at the particular locations. On the contrary, at $x/D = 2.0$, the flow velocity was modified for all three cases, where at this particular location the vortex formation is strongly detected for all treated and untreated cylinders. The delay in the formation of vortex is clear in the result for the porous case where V/U_o profiles are steeper in the case of porous relative to solid cylinder at $x/D = 1.5$ and further downstream.

A negative velocity region can also be seen clearly in the case of square cylinder at all locations. A contrary explanation is that, the profile with top hat behaviour can only be seen for the porous cases in the near wake which then change to fully developed wake further downstream. This explains that the recirculation region has already happened for solid square at very near wake. It is also observed that the momentum deficit of the porous cases in the near wake ($x/D = 0.5$ and $x/D = 1.0$) is smaller than that of rigid case, but larger in the far wake which is similar to the circular cylinder profile. The recirculation in the case of solid cylinder occurs earlier as the rigid profile becomes narrow at $x/D = 0.5$ in the negative velocity region. The recirculation region can also be seen clearly for the case of porous 20 PPI at the last location ($x/D = 3.0$) while the other two cases have shorten the recirculation region which also agrees with the results obtained in Fig. 10.

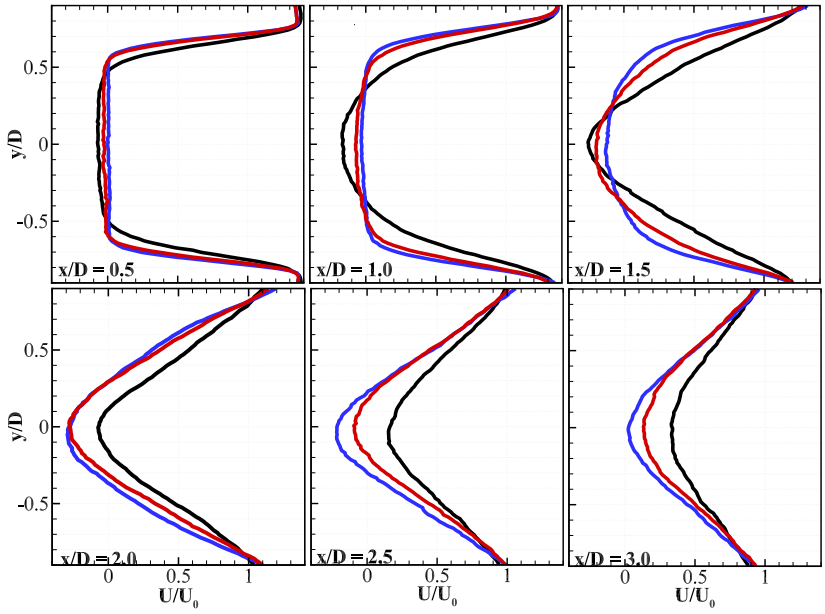

Figure 13: Mean U velocity components in the wake of the circular cylinder. *Black line: Solid; Blue line: Porous 25 PPI; Red line: Porous 80 PPI*

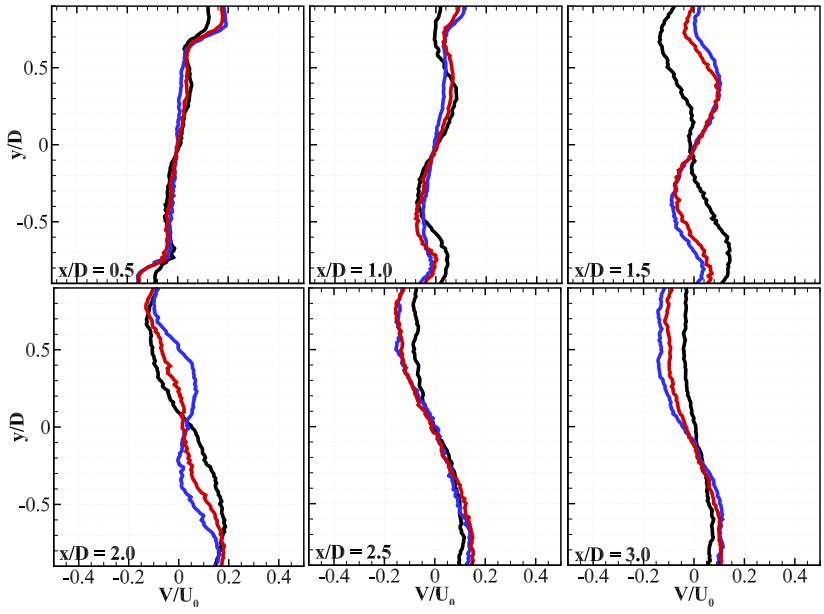

Figure 14: Mean V velocity components in the wake of the circular cylinder. *Black line: Solid; Blue line: Porous 25 PPI; Red line: Porous 80 PPI*

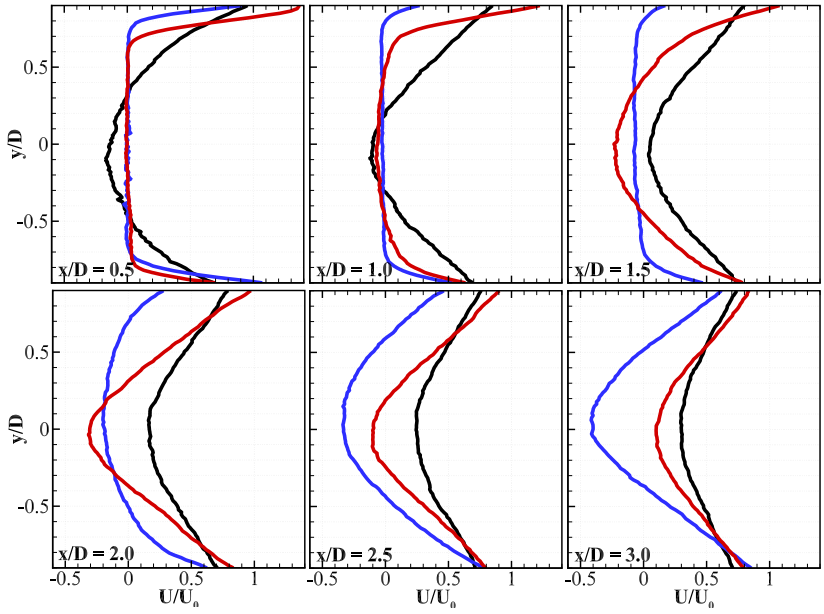

Figure 15: Mean U velocity components in the wake of the square cylinder. *Black line: Solid; Blue line: Porous 25 PPI; Red line: Porous 80 PPI*

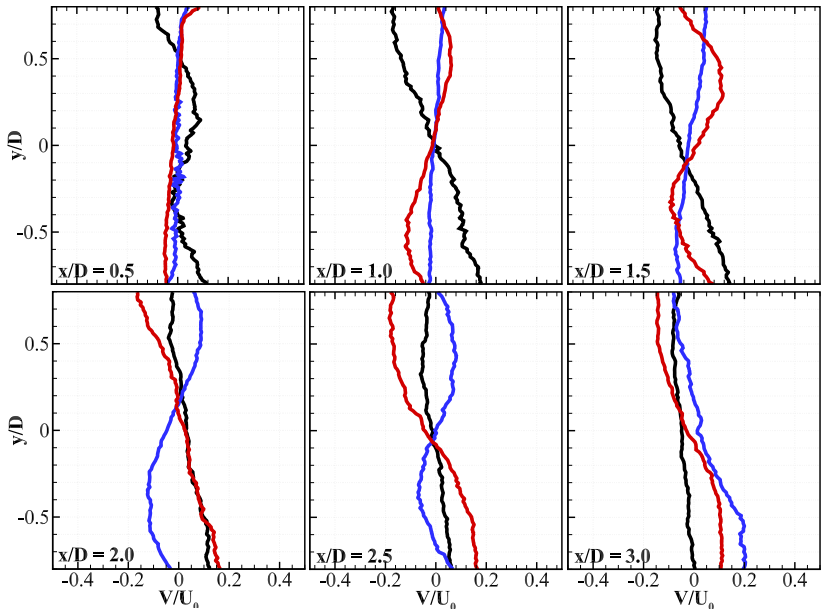

Figure 16: Mean V velocity components in the wake of the square cylinder. *Black line: Solid; Blue line: Porous 25 PPI; Red line: Porous 80 PPI*

C. Wake Energy Content

1. TKE contour plot for circular and square cylinders

To better understand the wake development and the effect of porous treatment, Figs. 17 and 18 are presented to show the dimensionless turbulence kinetic energy results in the wake. Both the figures show the TKE contour plots for both circular and square cylinders, respectively. It is clear that the TKE has been significantly reduced in the near wake by the effect of porous treated cylinders. Figure 17 also shows that the flow is much more two dimensional than the solid circular cylinder. It is apparent that the turbulence level is much higher for the case of solid square cylinder, shown in Fig. 18 (a). However, for the treated cylinders, the turbulence level have been reduced significantly in the near wake and has a much less energy in the far wake.

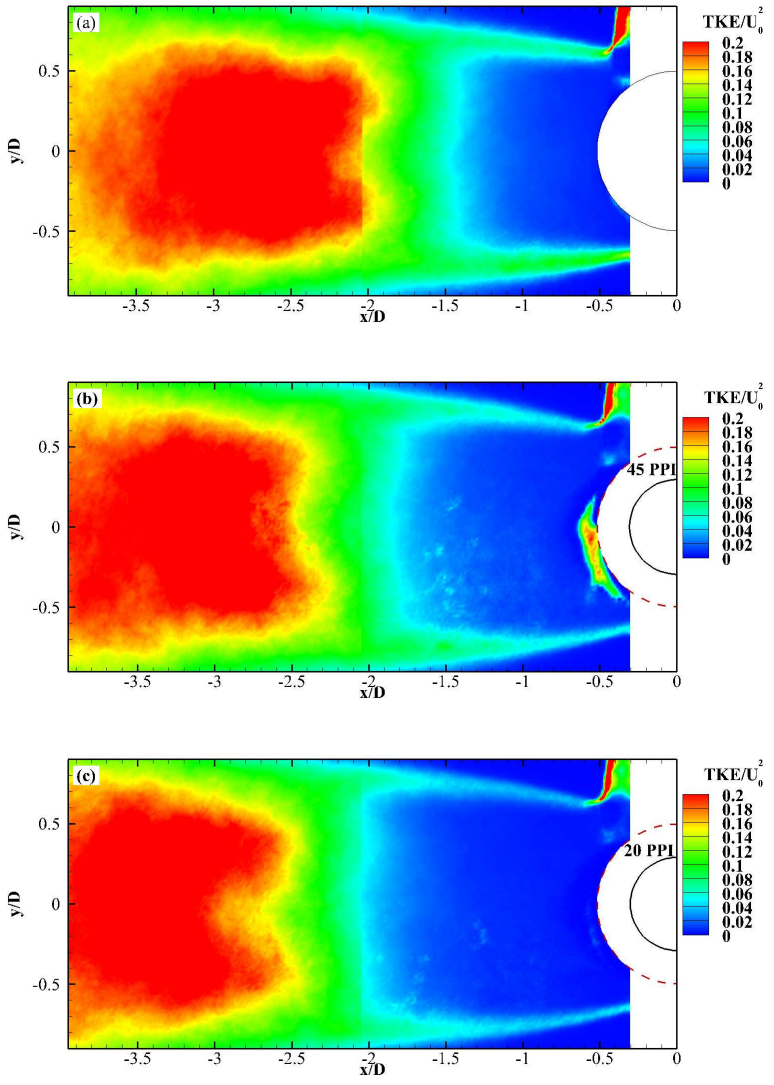

Figure 17: Time-averaged Turbulent Kinetic Energy (TKE) streamline topology for (a) a solid circular cylinder, (b) a circular cylinder covered with 45 PPI porous layer and (c) a circular cylinder covered with 25 PPI porous layer, at U_o =20 ms^{-1}.

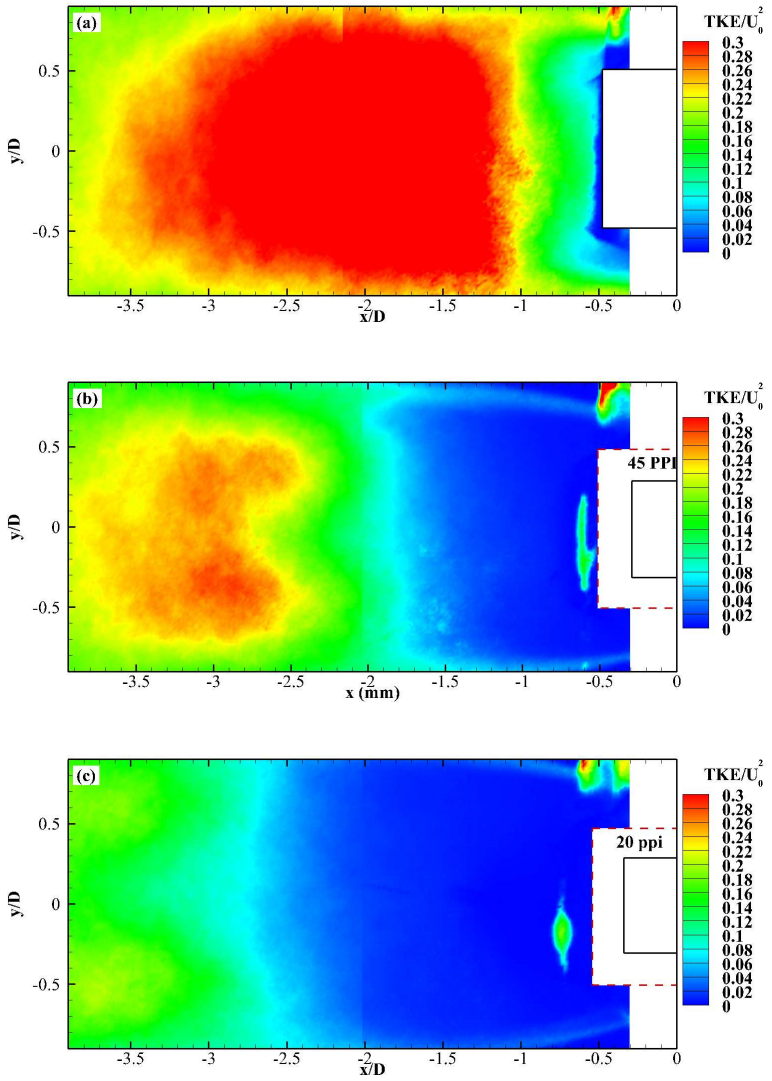

Figure 18: Time-averaged Turbulent Kinetic Energy (TKE) streamline topology for (a) a solid square cylinder, (b) a square cylinder covered with 45 PPI porous layer and (c) a square cylinder covered with 25 PPI porous layer, at U_o =20 ms^{-1}.

D. Reynold Shear Stresses (RSS)

To better understand the behaviour of the turbulent structures within the wake, the Reynold shear stress results are presented in Figs. 19 and 20 for circular and square cylinders, respectively. The variation of the time-averaged shear stresses ($\overline{u'v'}/U_o^2$), can be observed visually through the contour plot in Figs. 19 and 20. It is clear that the shear stress distribution is symmetrical along the wake centerline for all cases. Similarly observed before, the porous treated cylinder cases have significantly reduced the shear stress at the near wake. This is due to the suppression of vortex shedding and elongation of the vortex formation region observed in the earlier result.

It is clear from Fig. 19 that the eddy shearing stress component ($\overline{u'v'}/U_o^2$) for all cases have almost zero values at $x/D = 0.5$ and the treated cylinders continue to have constant zero values at $x/D = 1.0$. Similar to previous results, the vortices are effectively eliminated in the near wake region. In contrast to solid cylinder, the RSS of the porous case increases at the farther downstream locations and becomes dominant at $x/D = 3.0$. This is yet due to the occurrence of high fluctuating velocity in that region, which is consistent with the results obtained in the TKE profile. The distribution of the eddy shearing stress ($\overline{u'v'}/U_o^2$) is

somehow different in Fig. 20 for the case of square cylinders. Consistent with the earlier observation, the vortices are completely eliminated in the case of porous treated cylinders at $x/D = 0.5$, $x/D = 1.0$ and $x/D = 2.0$ (for porous 25 PPI). At all the locations, the RSS for the solid cylinder is much greater than the treated cylinders, however its value drops to some extent at $x/D = 3.0$.

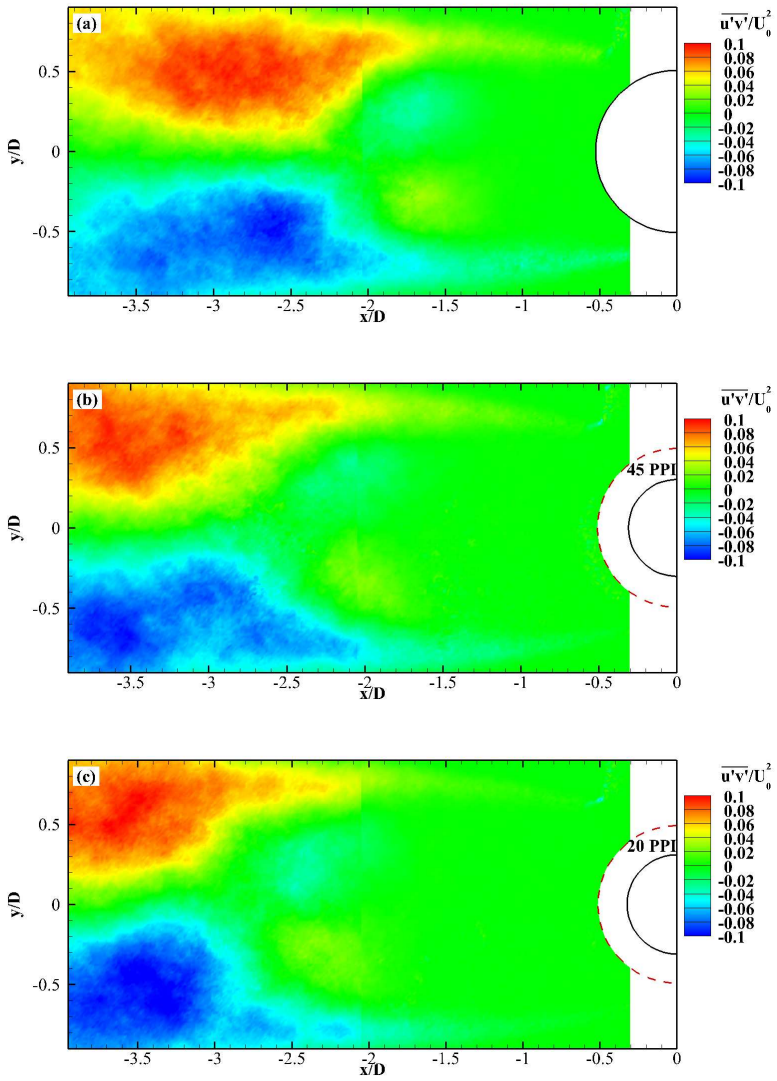

Figure 19: Time-averaged Reynolds shear stress term ($\overline{u'v'}/U_o^2$) streamline topology for (a) a solid circular cylinder, (b) a circular cylinder covered with 45 PPI porous layer and (c) a circular cylinder covered with 25 PPI porous layer, at U_o =20 ms^{-1}.

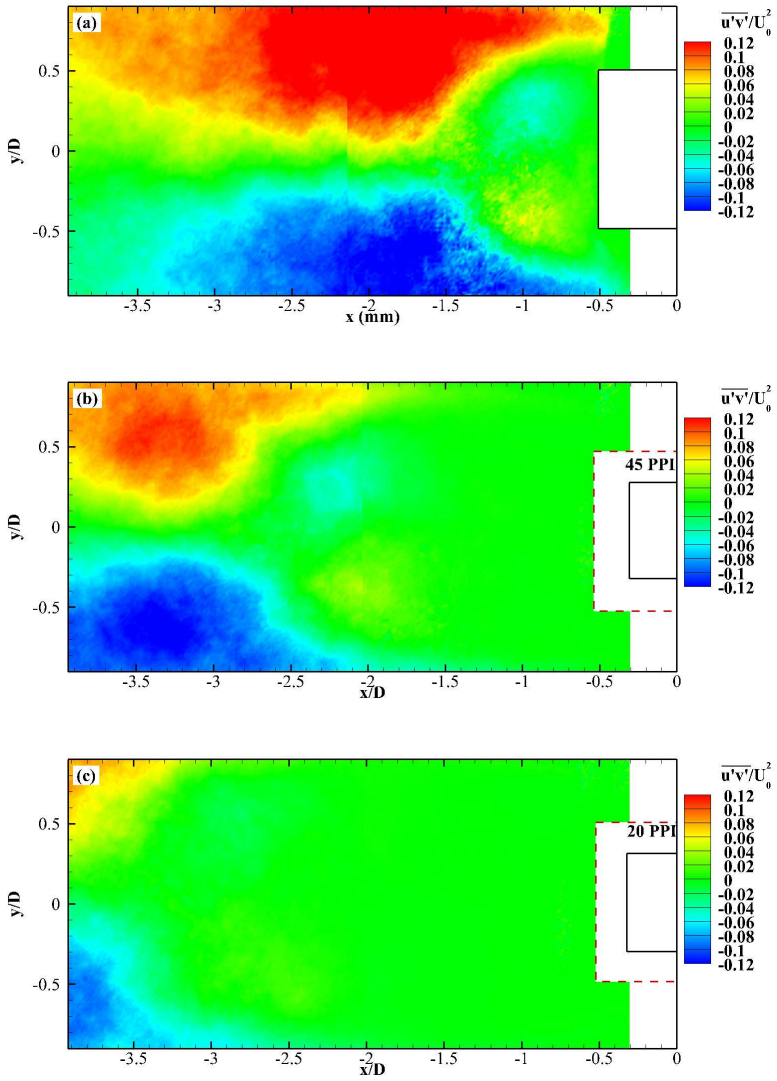

Figure 20: Time-averaged Reynolds shear stress term ($\overline{u'v'}/U_o^2$) streamline topology for (a) a solid square cylinder, (b) a square cylinder covered with 45 PPI porous layer and (c) a square cylinder covered with 25 PPI porous layer, at U_o =20 ms^{-1}.

E. Correlation Study

The statistical significance of flow structures within the wake flow field can be investigated using the two-point correlations of the instantaneous fluctuating velocity components. The correlation analysis has been computed in the streamwise, $f(r_1)$ locations downstream of the edge lip-line of upper cylinder using Eq. III at the Reynolds number of $Re_D = 10^5$, corresponding to the flow velocity of U_o =20 ms^{-1}. The measurement was carried out using two single hot-wire probes; one of the hot-wires has been fixed while the other one was traversed. The streamwise correlation test, $f(r_1)$ has been performed by locating the fixed probe at $x/D = 1.0$, while the second probe was traversed up to $\approx 4D$ downstream.

The streamwise correlation results for the both types of cylinders are presented in Figs. 21 and 22. It is clear that the use of porous treated cylinders have significant effect on the streamwise correlation in the wake. It is evident here that the porous treated circular cylinders are much more correlated in the near wake and decays less considerably compared to the solid cylinder and consistently becomes slightly negative correlated in the far wake. This trend can also be seen in the case of square cylinders, with solid cylinder being correlated to its maximum in the near wake and gradually decreases to slightly higher negative correlation

region. The negative correlation at $1 \lesssim x/D \lesssim 2$ for the case of solid circular cylinder occurred in the area where vortex formation is detected, *i.e.* the vortex formation can be seen in Fig. 9 (a). Conclusion can be drawn that the negative correlation region occurred in most of the cases is due to the presence of low and high shear regions in the wake flow. The indication of counter rotating vortex pairs in the correlation and anti-correlation region are more pronounced for solid cylinders in streamwise direction. One can deduce that the turbulence flow structures downstream of a porous treated cylinder are elongated in the streamwise direction.

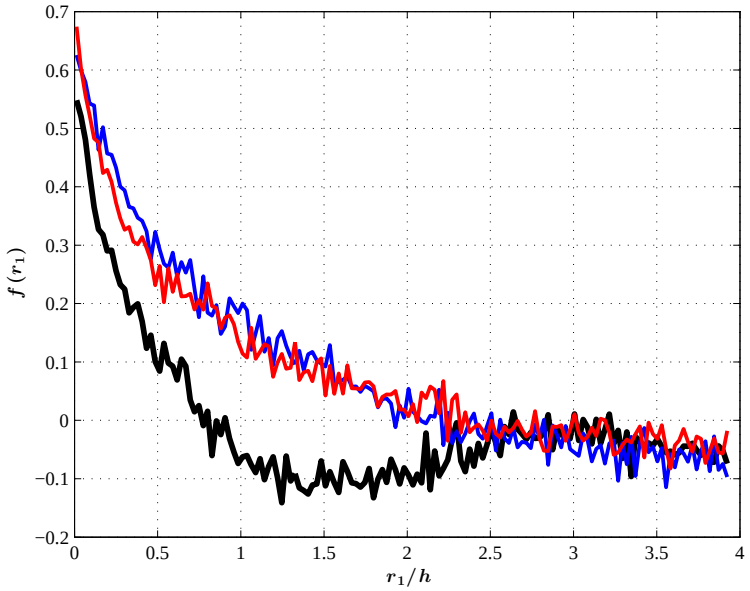

Figure 21: Streamwise correlation of the circular cylinder. *Black line: Solid; Blue line: Porous 25 PPI; Red line: Porous 80 PPI*

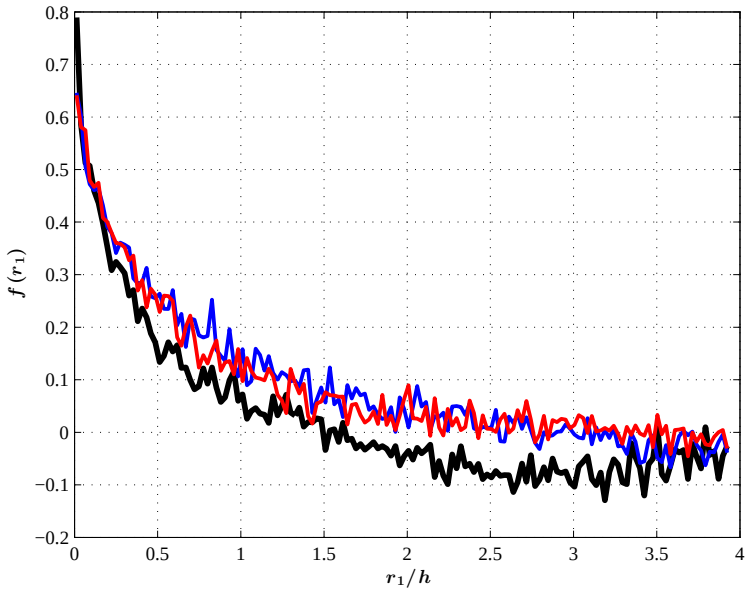

Figure 22: Streamwise correlation of the square cylinder. *Black line: Solid; Blue line: Porous 25 PPI; Red line: Porous 80 PPI*

V. Conclusions

The effect of porous materials on the flow and noise generation for circular and square cylinders have been investigated using force balance measurement, particle image velocimetry (PIV) and hot wire anemometry. It was found that there is a reduction in drag coefficient by all porous covers in the case of square cylinders and an increase in drag coefficient in the case of circular cylinder at high Reynolds number. The most effective porous is found to be those with higher permeability (20 PPI) and with larger porous thickness. It has also been shown that the lift fluctuations can be reduced significantly across the frequency range of interest using porous media. The PIV results have shown that the use of porous material results in moving of the main circulation area to further downstream. In the case of solid cylinder, the circulation occurs $2D$ downstream of the cylinder, while in the case of 25 PPI porous cover, the circulation moves to $3D$ or further downstream. The velocity profiles also show that the flow in the near wake is significantly stabilised and has very little shear stress. The turbulent kinetic energy and the shear stress results have shown that the flow energy content has been significantly reduced in the near wake and the flow is much more two dimensional than the solid case. The correlation studies revealed that the porous treatment has noticeably modified the correlation length of the velocity fluctuations in the streamwise directions. Thus, the present passive control method using porous media is found to be efficient and promising in controlling the noise generation mechanism and improving the aerodynamic performance.

Acknowledgments

The authors gratefully appreciate the technical discussion and support from Embraer S.A.

References

[1]Bhattacharyya, S. and Singh, A., "Reduction in drag and vortex shedding frequency through porous sheath around a circular cylinder," *International Journal for Numerical Methods in Fluids*, Vol. 65, No. 6, 2011, pp. 683–698.

[2]Chen, Z., Fan, B., Zhou, B., and Aubry, N., "Control of vortex shedding behind a circular cylinder using electromagnetic forces," *Modern Physics Letters B*, Vol. 19, No. 28n29, 2005, pp. 1627–1630.

[3]Li, Z., Navon, I., Hussaini, M., and Le Dimet, F.-X., "Optimal control of cylinder wakes via suction and blowing," *Computers & Fluids*, Vol. 32, No. 2, 2003, pp. 149–171.

[4]Homescu, C., Navon, I., and Li, Z., "Suppression of vortex shedding for flow around a circular cylinder using optimal control," *International Journal for Numerical Methods in Fluids*, Vol. 38, No. 1, 2002, pp. 43–69.

[5]Igarashi, T., "Drag reduction of a square prism by flow control using a small rod," *Journal of Wind Engineering and Industrial Aerodynamics*, Vol. 69, 1997, pp. 141–153.

[6]Lee, S.-J., Lee, S.-I., and Park, C.-W., "Reducing the drag on a circular cylinder by upstream installation of a small control rod," *Fluid dynamics research*, Vol. 34, No. 4, 2004, pp. 233–250.

[7]Lim, H.-C. and Lee, S.-J., "Flow control of a circular cylinder with O-rings," *Fluid Dynamics Research*, Vol. 35, No. 2, 2004, pp. 107–122.

[8]Lee, S.-J. and Kim, H.-B., "The effect of surface protrusions on the near wake of a circular cylinder," *Journal of Wind Engineering and Industrial Aerodynamics*, Vol. 69, 1997, pp. 351–361.

[9]

[10]Bearman, P. and Harvey, J., "Control of circular cylinder flow by the use of dimples," *AIAA journal*, Vol. 31, No. 10, 1993, pp. 1753–1756.

[11]Choi, J., *Mechanism of drag reduction by surface modification on a sphere: Dimples, roughness and trip wire*, Ph.D. thesis, Seoul Natl. Univ., Korea, 2006.

[12]Kunze, S. and Brücker, C., "Control of vortex shedding on a circular cylinder using self-adaptive hairy-flaps," *Comptes Rendus Mécanique*, Vol. 340, No. 1, 2012, pp. 41–56.

[13]Akilli, H., Sahin, B., and Tumen, N. F., "Suppression of vortex shedding of circular cylinder in shallow water by a splitter plate," *Flow Measurement and Instrumentation*, Vol. 16, No. 4, 2005, pp. 211–219.

[14]Ozono, S., "Flow control of vortex shedding by a short splitter plate asymmetrically arranged downstream of a cylinder," *Physics of Fluids*, Vol. 11, 1999, pp. 2928–2934.

[15]Lim, H.-C. and Lee, S.-J., "Flow control of circular cylinders with longitudinal grooved surfaces," *AIAA journal*, Vol. 40, No. 10, 2002, pp. 2027–2036.

[16]Sueki, T., Takaishi, T., Ikeda, M., and Arai, N., "Application of porous material to reduce aerodynamic sound from bluff bodies," *Fluid dynamics research*, Vol. 42, No. 1, 2010, pp. 015004.

[17]Sobera, M., Kleijn, C., and Van den Akker, H., "Subcritical flow past a circular cylinder surrounded by a porous layer," *Physics of Fluids (1994-present)*, Vol. 18, No. 3, 2006, pp. 038106.

[18]Bhattacharyya, S., Dhinakaran, S., and Khalili, A., "Fluid motion around and through a porous cylinder," *Chemical Engineering Science*, Vol. 61, No. 13, 2006, pp. 4451–4461.

[19]Gozmen, B., Fırat, E., Akilli, H., and Sahin, B., "Flow control behind a circular cylinder via a porous cylinder in deep water," *EPJ Web of Conferences*, Vol. 45, EDP Sciences, 2013, p. 01035.

[20]Jimenez, J., Uhlmann, M., Pinelli, A., and Kawahara, G., "Turbulent shear flow over active and passive porous surfaces," *Journal of Fluid Mechanics*, Vol. 442, 2001, pp. 89–117.

[21]Mimeau, C., Mortazavi, I., and Cottet, G.-H., "Passive flow control around a 2D semi-circular cylinder using porous media," .

[22]Vafai, K. and Kim, S.-J., "Analysis of surface enhancement by a porous substrate," *Journal of Heat Transfer*, Vol. 112, No. 3, 1990, pp. 700–706.

[23]Lim, H.-C. and Lee, S.-J., "Flow control of circular cylinders with longitudinal grooved surfaces," *AIAA journal*, Vol. 40, No. 10, 2002, pp. 2027–2036.

[24]Bruneau, C.-H., Mortazavi, I., and Gilliéron, P., "Passive control around the two-dimensional square back Ahmed body using porous devices," *Journal of Fluids Engineering*, Vol. 130, No. 6, 2008, pp. 061101.

[25]Bruneau, C.-H., Mortazavi, I., and Gilliéron, P., "Flow regularisation and drag reduction around blunt bodies using porous devices," *IUTAM Symposium on Flow Control and MEMS*, Springer, 2008, pp. 405–408.

[26]Bruneau, C.-H., Mortazavi, I., et al., "Control of vortex shedding around a pipe section using a porous sheath," *International Journal of Offshore and Polar Engineering*, Vol. 16, No. 02, 2006.

[27]Bruneau, C.-H., Mortazavi, I., et al., "Control of vortex shedding around a pipe section using a porous sheath," *International Journal of Offshore and Polar Engineering*, Vol. 16, No. 02, 2006.

[28]Naito, H. and Fukagata, K., "Numerical simulation of flow around a circular cylinder having porous surface," *Physics of Fluids*, Vol. 24, No. 11, 2012, cited By 5.

[29]Naito, H., Fukagata, K., and Obi, S., "MODIFICATION OF FLOW AROUND A CIRCULAR CYLINDER USING POROUS MEDIA," *Sixth International Symposium on Turbulence and Shear Flow Phenomena Seoul, Korea*, 2009.

[30]Liu, H., Azarpeyvand, M., Wei, J., and Qu, Z., "Tandem cylinder aerodynamic sound control using porous coating," *Journal of Sound and Vibration*, Vol. 334, 2015, pp. 190–201.

[31]Liu, H., Wei, J., and Qu, Z., "The Interaction of Porous Material Coating With the Near Wake of Bluff Body," *Journal of Fluids Engineering*, Vol. 136, No. 2, 2014, pp. 021302.

[32]Liu, H., Wei, J., and Qu, Z., "Prediction of aerodynamic noise reduction by using open-cell metal foam," *Journal of Sound and Vibration*, Vol. 331, No. 7, 2012, pp. 1483–1497.

[33]Szepessy, S. and Bearman, P., "Aspect ratio and end plate effects on vortex shedding from a circular cylinder," *Journal of Fluid Mechanics*, Vol. 234, 1992, pp. 191–217.

[34]Bearman, P. W. and Tombazis, N., "The effects of three-dimensional imposed disturbances on bluff body near wake flows," *Journal of Wind Engineering and Industrial Aerodynamics*, Vol. 49, No. 1, 1993, pp. 339–349.

[35]Roshko, A., "On the development of turbulent wakes from vortex streets," 1954.

[36]Berger, E. and Wille, R., "Periodic flow phenomena," *Annual Review of Fluid Mechanics*, Vol. 4, No. 1, 1972, pp. 313–340.

[37]Zdravkovich, M., "Flow around Circular Cylinders; Vol. I Fundamentals," *Journal of Fluid Mechanics*, Vol. 350, No. 1, 1997, pp. 377–378.

[38]Khashehchi, M., Abdi, I. A., Hooman, K., and Roesgen, T., "A comparison between the wake behind finned and foamed circular cylinders in cross-flow," *Experimental Thermal and Fluid Science*, Vol. 52, 2014, pp. 328–338.

[39]Abdi, I. A., Hooman, K., and Khashehchi, M., "A comparison between the separated flow structures near the wake of a bare and a foam-covered circular cylinder," *Journal of Fluids Engineering*, Vol. 136, No. 12, 2014, pp. 121203.

[40]Yoo, S. P. and Lee, D. Y., "Time-delayed phase-control for suppression of the flow-induced noise from an open cavity," *Applied Acoustics*, Vol. 69, No. 3, 2008, pp. 215–224.

[41]Lyu, B., Azarpeyvand, M., and Sinayoko, S., "Prediction of noise from serrated trailing edges," *Journal of Fluid Mechanics*, Vol. 793, 4 2016, pp. 556–588.

[42]Gruber, M., Azarpeyvand, M., and Joseph, P. F., "Airfoil trailing edge noise reduction by the introduction of sawtooth and slitted trailing edge geometries," *integration*, Vol. 10, 2010, pp. 6.

[43]Azarpeyvand, M., Gruber, M., and Joseph, P. F., "An analytical investigation of trailing edge noise reduction using novel serrations," *19th AIAA/CEAS Aeroacoustic Conference*, 2013, pp. 27–29.

[44]Sinayoko, S., Azarpeyvand, M., and Lyu, B., "Trailing edge noise prediction for rotating serrated blades," *20th AIAA/CEAS Aeroacoustics Conference*, 2014, pp. 16–20.

[45]Liu, X., Azarpeyvand, M., and Theunissen, R., "Aerodynamic and Aeroacoustic Performance of Serrated Airfoils," *21st AIAA/CEAS Aeroacoustics Conference*, 2015, p. 2201.

[46]Ai, Q., Azarpeyvand, M., Lachenal, X., and Weaver, P. M., "Aerodynamic and aeroacoustic performance of airfoils with morphing structures," *Wind Energy*, 2015.

[47]Ai, Q., Weaver, P., and Azarpeyvand, M., "Design optimization of a morphing flap device using variable stiffness materials," *24th AIAA/AHS Adaptive Structures Conference*, 2016, p. 0816.

[48]Stansby, P., "The effects of end plates on the base pressure coefficient of a circular cylinder," *Aeronautical Journal*, Vol. 78, 1974, pp. 36.

[49]Fox, T. and West, G., "On the use of end plates with circular cylinders," *Experiments in Fluids*, Vol. 9, No. 4, 1990, pp. 237–239.

[50]West, G. and Apelt, C., "The effects of tunnel blockage and aspect ratio on the mean flow past a circular cylinder with Reynolds numbers between 10 4 and 10 5," *Journal of Fluid Mechanics*, Vol. 114, 1982, pp. 361–377.

[51]Timmins, B. H., Smith, B. L., and Vlachos, P. P., "Automatic particle image velocimetry uncertainty quantification," *ASME 2010 3rd Joint US-European Fluids Engineering Summer Meeting collocated with 8th International Conference on Nanochannels, Microchannels, and Minichannels*, American Society of Mechanical Engineers, 2010, pp. 2811–2826.

[52]A/S, D. D., *Dantec Dynamics StreamWare Pro Installation and User Guide*, 5.11.00.14., 9040U4931, 2013.

[53]Darcy, H., "1856, Les Fontaines Publiques de la Ville de Dijon, Victor Dalmont, Paris," .

[54]Hufnagel, K. and Schewe, G., "Force and moment measurement," *Springer Handbook of Experimental Fluid Mechanics*, Springer, 2007, pp. 563–616.

[55]Bhattacharyya, S. and Singh, A., "Reduction in drag and vortex shedding frequency through porous sheath around a circular cylinder," *International Journal for Numerical Methods in Fluids*, Vol. 65, No. 6, 2011, pp. 683–698.

[56]Bruneau, C.-H. and Mortazavi, I., "Passive control of the flow around a square cylinder using porous media," *International Journal for Numerical Methods in Fluids*, Vol. 46, No. 4, 2004, pp. 415–433.

[57]Bearman, P., "Investigation of the flow behind a two-dimensional model with a blunt trailing edge and fitted with splitter plates," *Journal of Fluid Mechanics*, Vol. 21, No. 02, 1965, pp. 241–255.